

A new small-angle X-ray scattering set-up on the crystallography beamline I711 at MAX-lab

M. Knaapila,^{a,‡} C. Svensson,^a J. Barauskas,^{b,c} M. Zackrisson,^b S. S. Nielsen,^d K. N. Toft,^e B. Vestergaard,^e L. Arleth,^f U. Olsson,^b J. S. Pedersen^g and Y. Cerenius^{a,*}

^aMAX-lab, Lund University, POB 118, SE-22100 Lund, Sweden, ^bPhysical Chemistry 1, Center for Chemistry and Chemical Engineering, Lund University, POB 124, SE-22100 Lund, Sweden, ^cInstitute of Biochemistry, Mokslininku 12, LT-08662 Vilnius, Lithuania, ^dDanish Technical University, DK-2800 Lyngby, Denmark, ^eDepartment of Medicinal Chemistry, University of Copenhagen, DK-2100 Copenhagen, Denmark, ^fDepartment of Natural Sciences, University of Copenhagen, DK-1871 Fredriksberg, Denmark, and ^gDepartment of Chemistry and iNANO Interdisciplinary Nanoscience Center, University of Aarhus, DK-8000 Aarhus C, Denmark. E-mail: yngve.cerenius@maxlab.lu.se

A small-angle X-ray scattering (SAXS) set-up has recently been developed at beamline I711 at the MAX II storage ring in Lund (Sweden). An overview of the required modifications is presented here together with a number of application examples. The accessible q range in a SAXS experiment is 0.009–0.3 Å⁻¹ for the standard set-up but depends on the sample-to-detector distance, detector offset, beamstop size and wavelength. The SAXS camera has been designed to have a low background and has three collinear slit sets for collimating the incident beam. The standard beam size is about 0.37 mm × 0.37 mm (full width at half-maximum) at the sample position, with a flux of 4×10^{10} photons s⁻¹ and $\lambda = 1.1$ Å. The vacuum is of the order of 0.05 mbar in the unbroken beam path from the first slits until the exit window in front of the detector. A large sample chamber with a number of lead-throughs allows different sample environments to be mounted. This station is used for measurements on weakly scattering proteins in solutions and also for colloids, polymers and other nanoscale structures. A special application supported by the beamline is the effort to establish a micro-fluidic sample environment for structural analysis of samples that are only available in limited quantities. Overall, this work demonstrates how a cost-effective SAXS station can be constructed on a multipurpose beamline.

1. Introduction

Small-angle X-ray scattering (SAXS) (Pedersen, 2002; Svergun & Koch, 2003) is a well established method for obtaining structural information on the nanometer length scale. Beamlines dedicated to SAXS are becoming standard at synchrotron facilities and are described in numerous articles (see, for example, Abernathy *et al.*, 1998; Amenitsch *et al.*, 1997; Borsboom *et al.*, 1998; Fujisawa *et al.*, 2000; Haubold *et al.*, 1989; Lai *et al.*, 2005; Narayanan *et al.*, 2001; Paris *et al.*, 2007; Roessle *et al.*, 2007; Roth *et al.*, 2006; Yamamoto *et al.*, 1998). Over the last decade the interest in SAXS from the structural biology community has increased, partly as a result

of significant improvements of data analysis methods, introduced by Svergun and co-workers (Kozin & Svergun, 2001; Svergun, 1992, 1999; Svergun & Koch, 2002; Svergun *et al.*, 1988). Correspondingly, the user community is rapidly increasing and the demand for synchrotron beam time is growing. As a response to this growing demand, several dedicated high-flux SAXS beamlines are being commissioned at new third-generation synchrotron sources. As a supplement to these efforts, a quick and cost-effective way to increase the number of available SAXS facilities is to convert existing beamlines to SAXS or to add SAXS set-ups on multipurpose beamlines (Cernik *et al.*, 2004; Krywka *et al.*, 2007).

Beamline I711 of the 1.5 GeV storage ring MAX II at MAX-lab (Lund University, Sweden) was initially designed for crystallography (Cerenius *et al.*, 2000) but a major part of

[‡] Present address: Institute for Energy Technology, NO-2027 Kjeller, Norway.

Table 1

Essential parameters characterizing beamline I711 of MAX II.

Energy range (SAXS)	8–15 keV (0.8–1.6 Å)
Energy resolution	$\Delta E/E \approx 10^{-3}$
Focusing mirror	Cylindrical
Monochromator	Si(111) asymmetrically cut 7°
Flux† after a 0.3 mm slit at sample position	10^{11} photons s^{-1} (at 1.1 Å)

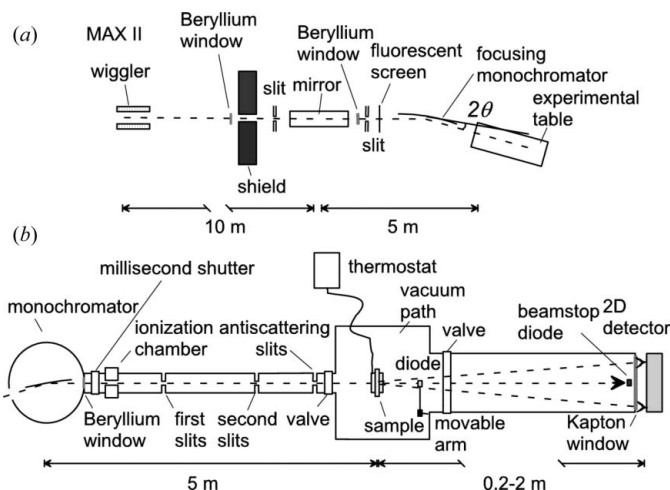
† Note that the careful collimation needed for a successful SAXS experiments limits the flux (see Table 2).

the available beam time is presently used for SAXS experiments. In this article we demonstrate how a competitive low-background SAXS set-up can be constructed on a multi-purpose crystallography beamline. The design has been inspired by a low-background instrumentation using a home source as described by Pedersen (2004). The SAXS instrument on I711 allows facile measurements of weakly scattering biomolecules and of ordered and uncorrelated colloids and polymers. Below we also present a selection of application examples. A special application supported by the beamline is a micro-fluidic sample environment (Toft *et al.*, 2008) for structural analysis of samples only available in very limited quantities.

2. Layout and instrumental components

The beamline I711 is described in detail elsewhere (Cerenius *et al.*, 2000). Its most important parameters are summarized in Table 1. The modifications for hosting SAXS experiments involve so far only the configuration inside the experimental hutch, downstream from the monochromator. The beamline is still used for small-molecule crystallography and powder-diffraction experiments part of the time. This limits the possibility of modifying the optics to make it even more suitable for SAXS measurements. Such modifications could include for example a larger bandwidth monochromator for increased flux. The time to switch from one experimental set-up to another is approximately one working day and typically carried out during the weekly machine day of the MAX II ring. Therefore, by scheduling beam time for each set-up on a weekly basis, the switches do not significantly lower the capacity of the beamline.

Fig. 1(a) shows a schematic top view of the layout of the beamline and Fig. 1(b) shows the SAXS set-up mounted on the 2θ arm. The most important design criteria of the SAXS set-up were low background and careful collimation of the incoming X-ray beam since these properties are crucial for weakly scattering samples. For collimation of the incoming beam a three-pinhole configuration is used (Pedersen, 2002), here achieved by three sets of slits (JJ-X-ray, Denmark) situated between the monochromator and the sample. The two first sets of slits, located at a distance of 1.6 and 2.85 m from the monochromator, are used to define the size and reduce the beam divergence. To have high flux, the beam is focused on the detector; however, the collimation is entirely determined by the slits. The sizes of the two first slits are chosen as $0.35 \text{ mm} \times 0.35 \text{ mm}$ (slit 1) and $0.30 \text{ mm} \times 0.30 \text{ mm}$ (slit 2),

**Figure 1**

Top-view sketch of (a) the I711 beamline and (b) SAXS station at I711 beamline. Not to scale.

resulting in a reduction of the beam intensity of close to a factor of 20 compared with the beam intensity with wide open slits. The third set of slits is located as close to the sample as possible at a distance of 0.66 m from slit 2 and used as guard slits thus just touching the beam defined by the first two slits. The guard slits minimize any parasitic scattering from the previous slits and their size is set by the maximum width of the beam ($0.62 \text{ mm} \times 0.62 \text{ mm}$). The FWHM of the beam at the sample position is $0.37 \text{ mm} \times 0.37 \text{ mm}$. The beamstop has to cover the high-background region on the detector which is defined by the most divergent rays that pass slit 2 and the guard slit. At a distance of 1.5 m from the sample, the maximum size is $2.8 \text{ mm} \times 2.8 \text{ mm}$, and to cover this a circular beamstop of diameter 4.0 mm is used. Note that beamstops of varying sizes are available. To reduce the background, the whole collimation and scattering paths are in vacuum with only two windows, the first one close to the monochromator, just after the shutter and ionization chamber, and the second one between the beamstop and the detector (Fig. 1b).

Fig. 2(a) shows a side view of the latter parts of the SAXS set-up. The sample vacuum chamber, Fig. 2(b) (Molecular Metrology Inc., today Rigaku), originally equipped with an ample amount of lead-throughs, vertical sample positioning and a beam-stop, was further improved with a number of add-ons (supplied by JJ-X-ray, Denmark), improving the accuracy regarding sample positioning and beam monitoring. For solution samples, sealed capillaries are typically used, similar to those used for the Kratky/SAXSess Camera (Anton Paar). The capillaries vary slightly in size so the background of weakly scattering samples has to be determined separately for each capillary. The capillaries are mounted in a six-position holder thermostated by a water-circulation bath (Julabo), Fig. 2(c). To increase the accuracy of the positioning of the capillary holder a linear encoder with $1 \mu\text{m}$ resolution was added to the vertical translation stage. Other sample environments, including users' own, such as flow-cells, microchips or cryostats, can be added. Alternatively, other sample holders

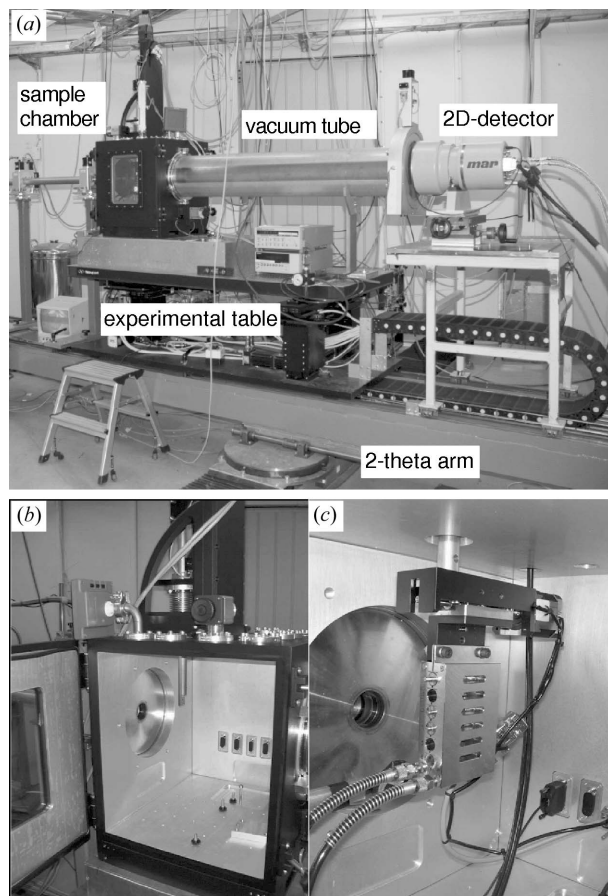


Figure 2
 (a) The SAXS station inside the experimental hutch at I711, (b) the sample chamber and (c) the thermostated sample holder with sealed capillaries.

may be mounted in front of the sample chamber, but then the X-ray beam may have to pass through air for some small distance. Two valves inserted immediately prior to and after the cubic sample chamber allow for selected ventilation of the sample chamber allowing for manipulation of samples. If these are not present, repeated and rapid ventilations would endanger the accuracy of the slit settings and beamstop position and significantly increase the time needed for sufficient evacuation.

The scattering data are measured using a 165 mm MarCCD detector (Marresearch). The sample-to-detector distance as well as the collimation length can be varied with a modular tube system. To change the sample-to-detector distance takes a few hours and includes refocusing of the incoming X-ray beam in the horizontal direction by changing the bending of the monochromator crystal. The vertical focusing is determined by the mirror that is situated 5 m upstream of the monochromator and is usually not affected by minor changes in the sample-to-detector distance. As already mentioned, a typical setting is a sample-to-detector distance of 1.5 m. This, in combination with a beam stop of 4 mm and a CCD detector with 165 mm diameter, results in an experimentally determined q range of 0.009 to 0.3 \AA^{-1} at a wavelength of 1.1 Å.

Table 2
 Parameters characterizing two typical settings of the SAXS station at I711 of MAX II.

	Setting I	Setting II
Beam size (FWHM)	0.37 mm × 0.37 mm	~0.22 mm × 0.22 mm
Flux (1.1 Å)	4×10^{10} photons s ⁻¹	9×10^9 photons s ⁻¹
Beamstop diameter	4 mm	1.8 mm
Sample–detector distance	1.5 m	1.5 m
Measurable q range	0.009–0.30 Å ⁻¹	0.0035–0.30 Å ⁻¹
Detectable structure	2–70 nm	2–140 nm

The parameters of two routinely used settings are compiled in Table 2.

The studies of weakly scattering samples require an accurate beam intensity monitoring system in order to allow proper normalization and background subtraction. In the normal experimental procedure the primary beam intensity is measured by an Oxford Danfysik IC *Plus* ion chamber that is placed before the slits (*cf.* Fig. 1*b*). This measurement is normally only used for beamline diagnostics. The beam decay and transmittance is measured by a Hamamatsu semi-conducting diode that is placed just after the sample and is automatically moved into the beam immediately before and after the sample exposure. When a succession of sample diode readings is plotted against time, the values vary only 0.5% from the curve expected because of ring current decay. This variation does not only account for the instabilities in diode readings but for all instabilities of the instrument, except detector noise. There are also photodiodes mounted inside the different beamstops, but the small active area of these make them very sensitive to small fluctuations of the beam position, and the readings have been shown to be less stable than those from the much larger sample diode. The beamstop diode is, however, a valuable tool for alignment purposes.

To partly compensate for the relatively high background of an integrating CCD detector compared with, for instance, a direct photon-counting detector, a shift procedure for the correction of the background has been adapted from Pontoni *et al.* (2002). A lead strip is attached such as to cover a part of the detector. Dark-current images are then normalized to the average count rates from the covered area. Such scaled dark-current images are subtracted from the non-covered area of all images. This procedure has proved to be efficient for removing the average remnant readout noise from each individual data frame.

Typical backgrounds of the SAXS set-up are shown in Fig. 3 with vacuum levels ranging from 2.9 mbar to 4.4×10^{-3} mbar evaluated from data images taken without any sample capillary in the beam path. A vacuum of 7×10^{-2} mbar is conveniently obtained, with a rotary pump, within a few minutes and decreases further down to 5×10^{-2} mbar in less than an hour. Once such vacuum levels have been reached, any changes in the background owing to variations in vacuum are negligible. In terms of scattering, this vacuum results in background levels corresponding to one-quarter of the scattering of 1.5 mm water, which is used as a standard for absolute calibration of intensities at the beamline.

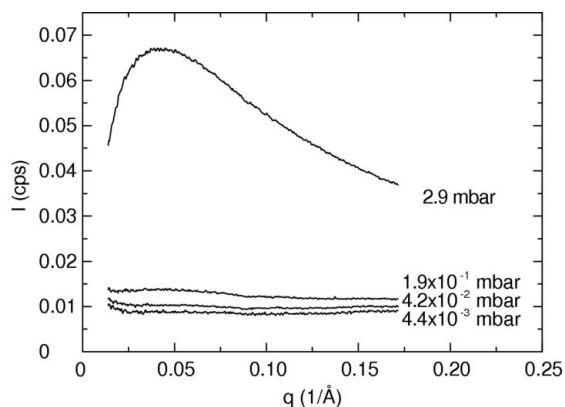


Figure 3
The background with different vacuum levels at the SAXS set-up on I711 as measured over 10 min. The numbers on the right correspond to the vacuum levels of the decreasing background level. The inherent background/bias of the applied CCD detector has been subtracted.

3. Software and data treatment

The hardware of the beamline optics and experimental set-up are controlled by *SPEC* (SPEC, Certified Scientific Software, Cambridge, MA., USA). A graphical user interface (GUI), Fig. 4, comprising also the necessary client software, communicates with *SPEC* in server mode. The GUI is developed at the beamline and written in Tcl/Tk. The GUI handles and displays all the scans of monochromator, slits, beamstop, sample holder and experimental table during alignment. This allows facile and user-friendly control of all beamline parameters and motors, counters *etc.* The GUI allows a convenient ‘spiral’ step scan for positioning the beamstop in the beam. This means that the motorized beamstop is scanned in a plane perpendicular to the beam, starting at the expected position. For each step the intensity is measured with the semi-conducting diode inside the beamstop. This scan continues until a local maximum is reached. The CCD detector can be set in remote mode and controlled *via* a socket from *SPEC* macros, which are in turn under GUI control. The GUI uses an

initialization file with automatic saving of up-to-date parameter values. There is also a log file with a summary function, which allows the user to easily review all the performed scans and measurements.

Prior to the sample measurements, the samples or sample capillaries are aligned by scanning the sample holder in the horizontal and vertical direction. Then a simple form is filled in to specify which samples to use, output file names, measurement times, temperatures *etc.* This complete list of measurements can also be set up to repeat at different times or different temperatures without further user intervention.

The GUI also has a viewer for the CCD images. Masks can be set in the form of rectangles, circles and polygons. Calibration and image integration are performed by a Fortran program accessed *via* a pipe. The wavelength of the experiment is calibrated with LaB₆ powder diffraction images taken with the detector at close distances to the sample, while beam center and distance calibration is performed with a reference sample, usually silver behenate, at the actual experiment sample–detector distance. For the data collection, the user can easily set up the GUI to integrate and display the experimental images as they are collected.

The SAXS evaluation part of the GUI offers both step-by-step and semi-automatic raw data processing. After setting up the integration parameters, the user can specify the image names of no-beam, empty capillary, water, solvent and sample exposures, or a subset of these. Data reduction is then automatic except for the estimation, in experiment units, of the flat scattering from water used for the absolute calibration. The lead-strip mask as described in §2 is routinely used for more accurate determinations of the detector background.

External software packages for raw data processing are also available for the convenience of the user and include *Fit2D* (Hammersley *et al.*, 1996) and a MATLAB-based *SAXSgui* originating from Molecular Metrology. A selection of data analysis software is also made available for users, for example the *ATSAS2.1* package (Konarev *et al.*, 2006).

Automated data reduction software is crucial for performing high-throughput chip-based experiments such as those that are carried out on I711 by the bioXTAS research project (<http://www.bioxtas.com/>). In these applications raw data processing (centering, masking, radial averaging, scaling and background subtraction) can be performed in an automatic mode with the bioXTAS *RAW* software. The latter program is written in Python/C++ and is fully open source (available upon request). During an experiment, bioXTAS *RAW* continuously searches for new incoming data. When a new two-dimensional data file is found, the software automatically performs an azimuthal average to one-dimensional format and plots the data. The two-dimensional to one-dimensional transformation includes q calibration, normalization of scattering intensity by transmission and by intensity of incoming beam, as well as error-bar calculation. Further data reduction in terms of, for example, background subtraction is carried out in the same software with a single click, and the final normalized and background-subtracted small-angle scattering data are output and saved in an ASCII format, fully

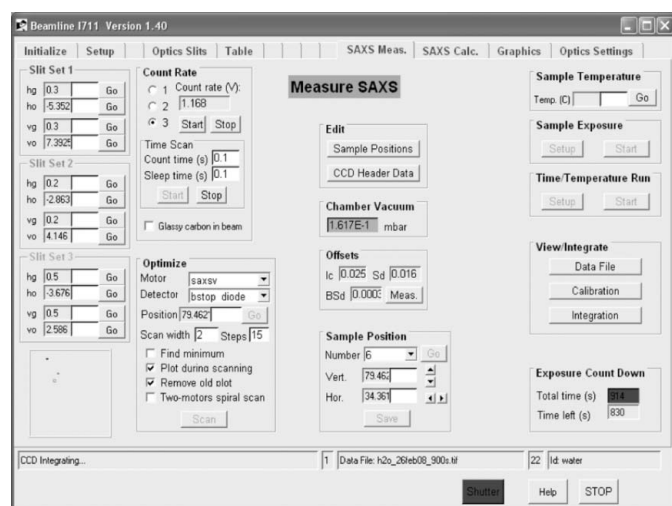


Figure 4
A snapshot of the GUI software at the I711 beamline.

compatible with, for example, the *ATSAS* software suite (Konarev *et al.*, 2006).

4. Application examples

Fig. 5 displays typical data of the standard samples as collected with a photon energy of 10 keV. Two common standard samples are routinely used in calibrating the new SAXS set-up. Silver behenate, a silver salt of a long-chain carboxylic acid ($\text{AgC}_{22}\text{H}_{43}\text{O}_2$) with $d_{001} = 58.380 \text{ \AA}$ (Huang *et al.*, 1993), is employed for the calibration of the instrument q range. Water is used for the absolute intensity calibration in terms of determining the differential cross section per unit volume of sample. The latter calibration can be performed semi-automatically by the in-house developed software (see §3) following standard procedures (Dreiss *et al.*, 2006; Orthaber *et al.*, 2000). In addition, a polyethylene sample, mutually calibrated in the group of J. S. Pedersen (Pedersen, 2004), is routinely employed as a secondary reference. Also shown is a measured form factor for dilute (1 wt%) polystyrene spheres in water (3030A Nanospheres, Dukes Scientific Corporation) after 20 min exposure at room temperature. These data

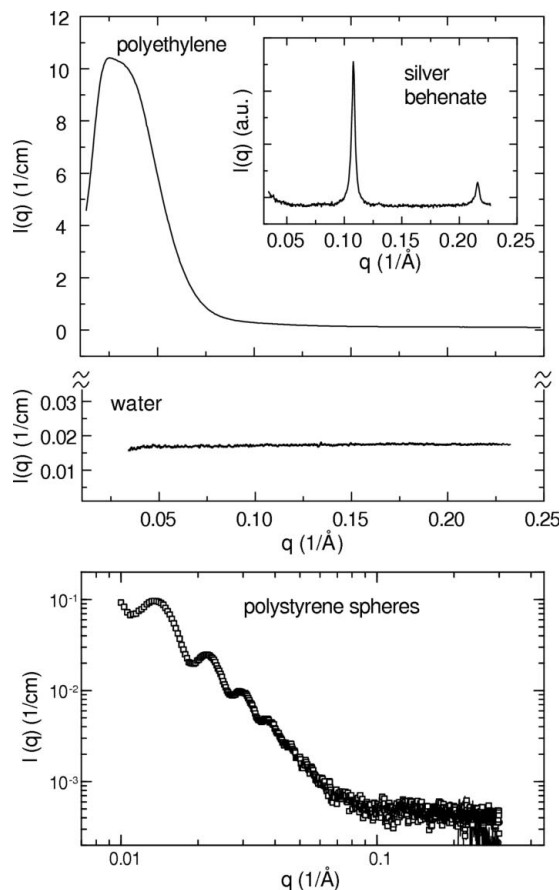


Figure 5 Upper panels: SAXS patterns of polyethylene and silver behenate collected at the SAXS station of the I711 beamline with a photon energy of 10 keV (1.2 Å). The polyethylene gives a maximum 10.4 cm^{-1} at 0.025 \AA^{-1} . Lower panel: SAXS pattern of colloidal polystyrene particles in water (1 wt%) as measured at the I711 beamline at MAX-lab (open squares). The average radius of the particles is 33 nm.

demonstrate that the SAXS station at I711 resolves the scattering of a sample known to be ill-suited for X-rays owing to low contrast.

As a demonstration of the capability of the instrument to capture the dynamic process of protein fibrillation, a sample of 30 mg ml^{-1} of α -lactalbumin in 75 mM Tris buffer at pH 8 was measured (Fig. 6). Protein fibrillation was induced by adding a protease from bacillus licheniformis which partially hydrolyses the lactalbumin and induces protein fibrillation. Measurements were performed in 5 min exposures during a 1 h fibrillation process, where the sample was left to hydrolyse and fibrillate in a cuvette at 323 K. Buffer background measurements were performed in between the sample measurements, but in another sample cell. The oscillation in the SAXS data showing up at around 0.04 \AA^{-1} already after 18 min is the clear signature of the formation of long hollow tubes with a cross-sectional diameter of about 20 nm as previously demonstrated (Graveland-Bikker *et al.*, 2006; Ipsen & Otte, 2007). These data show how the transition can be measured at the low- q part of the data.

As an interesting test of the new SAXS station we have performed scattering experiments on diluted protein samples in a 200 nL sample chamber on the bioXTAS chip as described by Toft *et al.* (2008). Measuring SAXS on dilute protein solutions is challenging because a relatively weak protein signal rides on top of a comparatively high buffer background signal. In order to obtain good quality data, extra attention must be devoted to minimizing the instrument background, including parasitic scattering and scattering from, for example, windows and air molecules in the flight path of the scattered beam. Likewise, accurate background subtractions including accurate transmission measurements are crucially important. Thus the ability to measure dilute protein solutions may be regarded as a benchmark for the general quality of a SAXS instrument. In this very application the samples are pumped

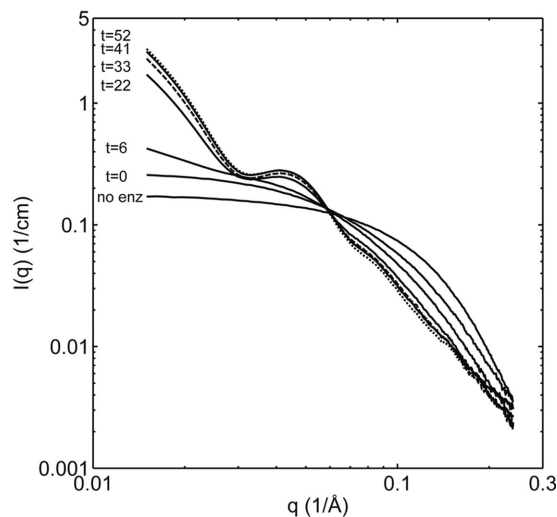


Figure 6 SAXS data measured at different times of the fibrillation process of 30 mg ml^{-1} of α -lactalbumin at 323 K. Indicated times are the start times of the X-ray exposure. The scattering curves at time t represent scattering from the sample in the time interval between t and $t + 5$ min.

into the sample chamber *via* fluidic lines without breaking vacuum and this hardware is set to work parallel to data acquisition. The benefit of applying small sample volumes of biological samples is obvious, as many biological samples are only available in limited amounts. Our aim is to be able to incorporate such a small-volume sample chamber both software- and hardware-wise so that this could be offered to future users. External users are until then offered a standard flow-through cell (Dubuisson *et al.*, 1997) kindly provided by the SWING beamline at Soleil. No significant evidence for radiation damage has been observed for any protein solution work at the beamline.

Apart from proteins the new station can be used in studies of uncorrelated polymer and colloid particles (Knaapila *et al.*, 2007; Popescu *et al.*, 2007). SAXS experiments have in these cases been complemented by other methods such as small-angle neutron scattering (SANS). Solution structures of stiff polyfluorenes belong to the prime examples amongst π -conjugated polymers. Fig. 7 illustrates characteristic SAXS data of a polyfluorene gel as measured at I711 and shows the use of the whole accessible q range. The corresponding SANS data as measured by the SANS instruments in Geesthacht (Stuhrmann *et al.*, 1995) and Budapest (Rosta, 2002) are shown for comparison. These kinds of polymers form sheetlike assemblies (or membranes) whose thicknesses are 1–3 nm and whose lateral dimensions cover the range 10–100 nm. The differences in the small-angle scattering stemming from the contrast difference between X-rays and neutrons allow detailed structural characterization of these sheets in the solution state. This represents an example where I711 data are successfully connected to neutron scattering data which alto-

gether have revealed the self-organized structure formation of polyfluorene systems (Knaapila *et al.*, 2007).

5. Remarks and outlook

Summarizing, we have constructed a cost-effective SAXS set-up with a user-friendly graphical interface for data acquisition and reduction at the crystallography beamline I711. The crystallography hardware can be turned into a SAXS set-up in one working day. Several measurements have been conducted to demonstrate its performance and usefulness in research on solutions of proteins, polymers and colloids. A special application, supported by the beamline, is the effort to establish a micro-fluidic sample environment for structural analysis of samples that are available in limited quantities. Around 50% of the total beam time of the multi-purpose beamline I711, corresponding to 25 user groups, was scheduled for SAXS in the first year of the station. The set-up is under constant improvement and the future developments will be directed by the user requirements. This report demonstrates how a beamline initially dedicated to crystallography can also host a low-background SAXS station.

The authors acknowledge funding from the Swedish Research Council, DANSYNC, the Danish Strategic Research Council (NABIIT contract No. 2106-05-0047), the Danish Medical Research Council, as well as EU-STREP FP6 project BIOSCOPE (contract No. NMP4-CT-2003-505211). C. L. P. Oliveira of the University of Aarhus is acknowledged for the mutual calibration of standards and fruitful discussions.

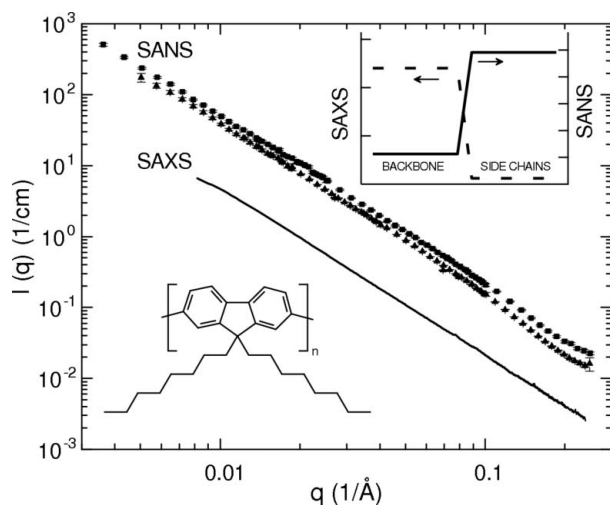


Figure 7
SAXS data of poly(9,9-dioctylfluorene) in methylcyclohexane as measured using the SAXS set-up on I711 (solid line). For comparison, also shown are corresponding SANS data as measured in deuterated solvent at the SANS-1 instrument at Geesthacht Neutron Facility (solid triangles), and the Yellow Submarine instrument at the Budapest Neutron Centre (solid squares). Insets illustrate the chemical structure of the polymer with backbone and side chains and their contrast difference between X-rays and neutrons, which is responsible for different intensity levels. For further details, see Knaapila *et al.* (2007).

References

- Abernathy, D. L., Grübel, G., Brauer, S., McNulty, I., Stephenson, G. B., Mochrie, S. G. J., Sandy, A. R., Mulders, N. & Sutton, M. (1998). *J. Synchrotron Rad.* **5**, 37–47.
- Amenitsch, H., Bernstorff, S., Kriechbaum, M., Lombardo, D., Mio, H., Rappolt, M. & Laggner, P. (1997). *J. Appl. Cryst.* **30**, 872–876.
- Borsboom, M., Bras, W., Cerjak, I., Detollenaere, D., Glastra van Loon, D., Goedtkindt, P., Konijnenburg, M., Lassing, P., Levine, Y. K., Munneke, B., Oversluisen, M., van Tol, R. & Vlieg, E. (1998). *J. Synchrotron Rad.* **5**, 518–520.
- Cerenius, Y., Ståhl, K., Svensson, L. A., Ursby, T., Oskarsson, Å., Albertsson, J. & Liljas, A. (2000). *J. Synchrotron Rad.* **7**, 203–208.
- Cernik, R. J., Barnes, P., Bushnell-Wye, G., Dent, A. J., Diakun, G. P., Flaherty, J. V., Greaves, G. N., Heeley, E. L., Helsby, W., Jacques, S. D. M., Kay, J., Rayment, T., Ryan, A., Tang, C. C. & Terrill, N. J. (2004). *J. Synchrotron Rad.* **11**, 163–170.
- Dréiss, C. A., Jack, K. S. & Parker, A. P. (2006). *J. Appl. Cryst.* **39**, 32–38.
- Dubuisson, J.-M., Decamps, T. & Vachette, P. (1997). *J. Appl. Cryst.* **30**, 49–54.
- Fujisawa, T., Inoue, K., Oka, T., Iwamoto, H., Uruga, T., Kumasaka, T., Inoko, Y., Yagi, N., Yamamoto, M. & Ueki, T. (2000). *J. Appl. Cryst.* **33**, 797–800.
- Graveland-Bikker, J. F., Fritz, G., Glatter, O. & de Kruijff, C. G. (2006). *J. Appl. Cryst.* **39**, 180–184.
- Hammersley, A. P., Svensson, S. O., Hanfland, M., Fitch, A. N. & Hausermann, D. (1996). *High Press. Res.* **14**, 235–248.

- Haubold, H.-G., Gruenhagen, K., Wagener, M., Jungbluth, H., Heer, H., Pfeil, A., Rongen, H., Brandenburg, G., Moeller, R., Matzerath, J., Hiller, P. & Halling, H. (1989). *Rev. Sci. Instrum.* **60**, 1943–1946.
- Huang, T. C., Toraya, H., Blanton, T. N. & Wu, Y. (1993). *J. Appl. Cryst.* **26**, 180–184.
- Ipsen, R. & Otte, J. (2007). *Biotech. Adv.* **25**, 602–605.
- Knaapila, M., Dias, F. B., Garamus, V. M., Almásy, L., Torkkeli, M., Leppänen, K., Galbrecht, F., Preis, E., Burrows, H. D., Scherf, U. & Monkman, A. P. (2007). *Macromolecules*, **40**, 9398–9405.
- Konarev, P. V., Petoukhov, M. V., Volkov, V. V. & Svergun, D. I. (2006). *J. Appl. Cryst.* **39**, 277–286.
- Kozin, M. B. & Svergun, D. I. (2001). *J. Appl. Cryst.* **34**, 33–41.
- Krywka, C., Sternemann, C., Paulus, M., Javid, N., Winter, R., Al-Sawalmih, A., Yi, S., Raabe, D. & Tolan, M. (2007). *J. Synchrotron Rad.* **14**, 244–251.
- Lai, Y. H., Sun, Y. S., Jeng, U., Huang, Y.-S., Song, Y. F., Dronyak, R., Tsang, K. L. & Liang, K. S. (2005). *Nucl. Instrum. Methods Phys. Res. B*, **238**, 205–213.
- Narayanan, T., Diat, O. & Bösecke, P. (2001). *Nucl. Instrum. Methods Phys. Res. A*, **467–468**, 1005–1009.
- Orthaber, D., Bergmann, A. & Glatter, O. (2000). *J. Appl. Cryst.* **33**, 218–225.
- Paris, O., Li, C., Siegel, S., Weseloh, G., Emmerling, F., Riesemeier, H., Erko, A. & Fratzl, P. (2007). *J. Appl. Cryst.* **40**, s466–s470.
- Pedersen, J. S. (2002). *Neutrons, X-rays and Light: Scattering Methods Applied to Soft Condensed Matter*, edited by P. Lindner and Th. Zemb. Amsterdam: North-Holland.
- Pedersen, J. S. (2004). *J. Appl. Cryst.* **37**, 369–380.
- Pontoni, D., Narayanan, T. & Rennie, A. R. (2002). *J. Appl. Cryst.* **35**, 207–211.
- Popescu, G., Barauskas, J., Nylander, T. & Tiberg, F. (2007). *Langmuir*, **23**, 496–503.
- Roessle, M. W., Klaering, R., Ristau, U., Robrahn, B., Jahn, D., Gehrman, T., Konarev, P., Round, A., Fiedler, S., Hermes, C. & Svergun, D. (2007). *J. Appl. Cryst.* **40**, s190–s194.
- Rosta, L. (2002). *Appl. Phys. A*, **74**, S52–S54.
- Roth, S. V., Döhrmann, R., Dommach, M., Kuhlmann, M., Kröger, I., Gehrke, R., Walter, H., Schroer, C., Lengeler, B. & Müller-Buschbaum, P. (2006). *Rev. Sci. Instrum.* **77**, 085106.
- Stuhrmann, H. B., Burkhardt, N., Dietrich, G., Jünemann, R., Meerwinck, W., Schmitt, M., Wadzack, J., Willumeit, R., Zhao, J. & Nierhaus, K. H. (1995). *Nucl. Instrum. Methods Phys. Res. A*, **356**, 124–132.
- Svergun, D. I. (1992). *J. Appl. Cryst.* **25**, 495–503.
- Svergun, D. I. (1999). *Biophys. J.* **76**, 2879–2886.
- Svergun, D. I. & Koch, M. H. J. (2002). *Curr. Opin. Struct. Biol.* **12**, 654–660.
- Svergun, D. I. & Koch, M. H. J. (2003). *Rep. Prog. Phys.* **66**, 1735–1782.
- Svergun, D. I., Semenyuk, A. V. & Feigin, L. A. (1988). *Acta Cryst.* **A44**, 244–250.
- Toft, K. N., Vestergaard, B., Nielsen, S. S., Snakenborg, D., Jeppesen, M. G., Jacobsen, J. K., Arleth, L. & Kutter, J. P. (2008). *Anal. Chem.* **80**, 3648–3654.
- Yamamoto, M., Kumasaka, T., Fujisawa, T. & Ueki, T. (1998). *J. Synchrotron Rad.* **5**, 222–225.